Clays and Clay Minerals, Vol. 66, No. 2, 114–126, 2018.

EFFECTS OF DYE SURFACE CONCENTRATION ON THE MOLECULAR AGGREGATION OF XANTHENE DYE IN COLLOIDAL DISPERSIONS OF MONTMORILLONITE

Tímea Baranyaiová[1] and Juraj Bujdák[1,2,*]

[1] Comenius University in Bratislava, Department of Physical and Theoretical Chemistry, Faculty of Natural Sciences, 842 15 Bratislava, Slovakia

[2] Institute of Inorganic Chemistry, Slovak Academy of Sciences, 845 36 Bratislava, Slovakia

Abstract—The molecular aggregation of organic dyes onto clay mineral particles is a very complex phenomenon including dye adsorption, the migration of dye molecules, rearrangement of initially formed aggregates, *etc*. Some details of this complex process are not yet fully understood. The objective of the present study was to understand the influence of dye surface concentration on the dynamic processes in dye molecular aggregation. A stopped-flow rapid mixing device was used for accurate measurements of the molecular aggregation of the cationic dye rhodamine 123 (R123) in montmorillonite (MntK) colloidal dispersions. The influence of dye surface concentration, which was changed by altering the ratio of the amount of R123 to the mass of MntK (n_{R123}/m_{MntK}), was examined in detail. Chemometric analysis was used to reconstruct the spectral matrix to obtain linearly uncorrelated spectral profiles of the major components and their concentrations at the respective reaction times. The conversion of isolated R123 cations into oblique J-aggregates (head-to-tail molecular assemblies) was observed over time and the existence of a J-dimers intermediate was hypothesized. The reaction kinetics followed a biphasic exponential function. An unexpected effect of dye surface concentration on R123 aggregation was observed: the initial formation of the molecular aggregates increased significantly with dye surface concentration, but an inverse trend was observed after longer reaction times. While dye aggregates were formed slowly at low dye loadings, systems with high R123/MntK ratios (n_{R123}/m_{MntK}) reached spectral stability after the first few seconds of the reaction. After longer reaction times, the greatest degree of dye aggregation was achieved in the dispersion of the lowest dye loading. Such a phenomenon is described for the first time. The results presented here are important for understanding the complex processes occurring in systems based on organic cations and clay minerals, and should be considered in the development of functional hybrid materials of dyes and nanoparticles with a layered structure.

Key Words—Chemometric Analysis, Metachromasia, Molecular Aggregates, Reaction Kinetics, Rhodamine 123, Smectite, UV-Vis Spectroscopy.

INTRODUCTION

The phenomenon of metachromasia, which is an apparent change in the color of certain dyes, was first observed by biologists in the staining of biological tissues (Holmes, 1926). Following the introduction of "exciton theory" (McRae and Kasha, 1958; Kasha *et al.*, 1965), metachromasia was described in terms of dye molecular aggregation. Although molecular aggregation has been investigated for a variety of systems, including concentrated solutions, interfaces, polyelectrolyte solutions, hybrid materials, *etc*., some aspects of this phenomenon are not fully understood.

After the first report on methylene blue (MB) metachromasia in a montmorillonite colloid (Bergmann and O'Konski, 1963), numerous reports on this topic were published. Clay minerals as substrates that promote metachromasia have very different properties (Cenens and Schoonheydt, 1988; Bujdák, 2006). Depending on the clay sample and the conditions used, various dye molecular assemblies could be formed. These include adsorbed, non-aggregated forms referred to as monomers, sandwich-type H-dimers and H-aggregates, head-to-tail J-aggregates, or aggregates with imperfect structure or variable sizes (Figure 1). The metachromatic responses of adsorbed dye molecules obviously reflect somehow the surface properties of the clay mineral particles. Various parameters have been investigated with respect to this phenomenon, such as the clay mineral type (López Arbeloa *et al.*, 1995; Bujdák *et al.*, 2001; Czímerová *et al.*, 2006), particle size (Miyamoto *et al.*, 2000; Bujdák *et al.*, 2002; Sartori *et al.*, 2011), composition and structure (Bujdák *et al.*, 2001; Czímerová *et al.*, 2006), swelling (Neumann *et al.*, 2002), type of exchangeable cations (Czímerová *et al.*, 2004), layer-charge density (Bujdák and Komadel, 1997; Bujdák *et al.*, 2001; Bujdák *et al.*, 2004) and location

* E-mail address of corresponding author:
juraj.bujdak@uniba.sk
DOI: 10.1346/CCMN.2018.064089

This paper was originally presented during the session 'NT-12. Photo- and optical functionalities of clay-based hybrid materials' during ICC 2017

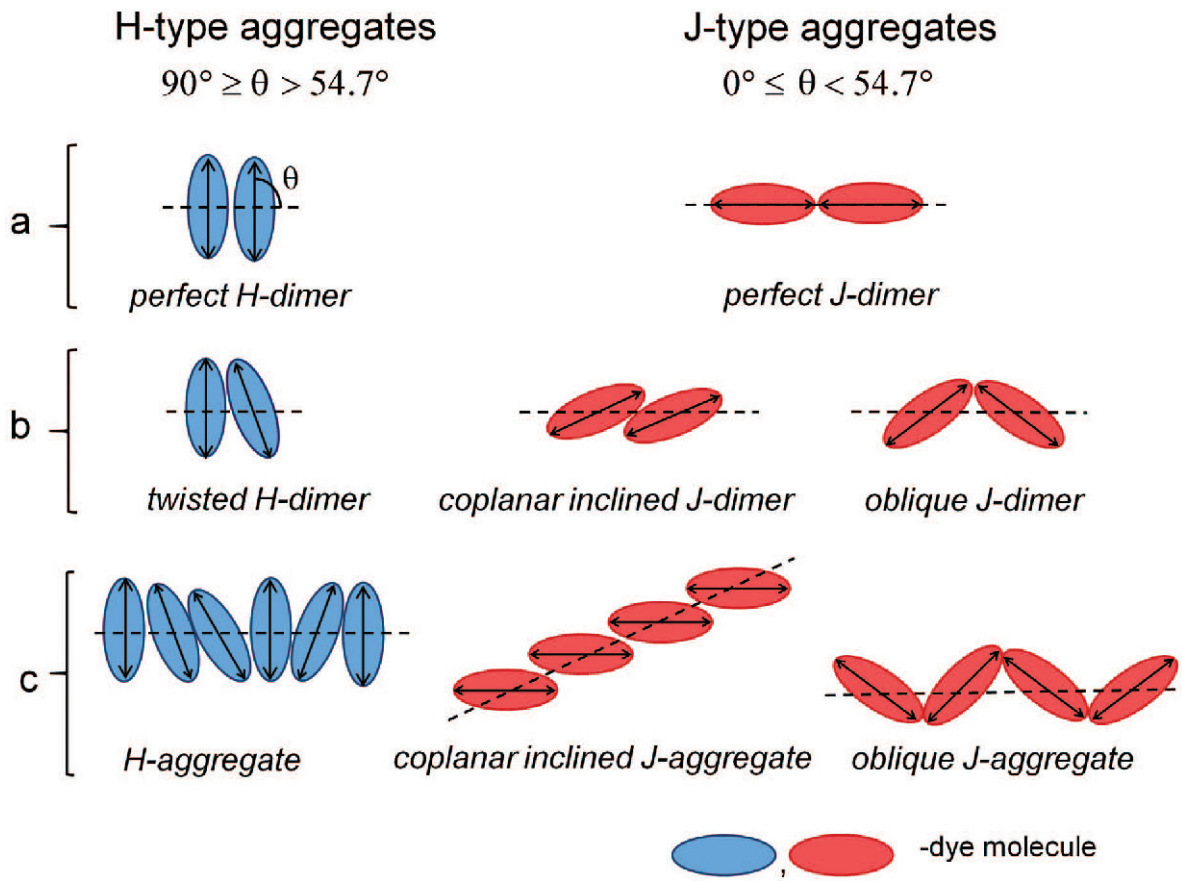

Figure 1. Schematic illustration of structural differences between H- and J-molecular aggregates: structurally perfect H- and J-dimers (a); structurally non-ideal H- and J-dimers with intermediate geometries (b); and higher H- and J-aggregates with imperfect structure (c). The slip angle (θ) corresponds to the angle between the main axes of the dye molecules (double-headed arrow) and the centerline of the interacting molecules in the aggregate (dashed line). The value range for the slip angle was given by McRae and Kasha (1958).

(Bujdák *et al.*, 2001; Jacobs and Schoonheydt, 2001; Epelde-Elezcano *et al.*, 2016), dye concentration (Schoonheydt and Heughebaert, 1992; Estevez *et al.*, 1993), and dye properties and molecular structure (Bujdák and Iyi, 2006; Czímerová *et al.*, 2009). Even very dilute, fully exfoliated and stable colloidal dispersions of smectite samples saturated with Na^+ or Li^+ ions could have very different properties to promote dye molecular aggregation.

The main contribution to current knowledge of this phenomenon was the discovery of the layer-charge effect on dye molecular aggregation (Bujdák and Komadel, 1997; Bujdák, 2006). The layer charge controls sensitively the distribution of counterions near the particle surface, mainly in the Stern layer. The distances between adjacent dye cations adsorbed on the particle surface are controlled by layer-charge distribution. The distribution of the layer charge affects the type and extent of the molecular aggregation of cationic dyes. Interestingly, a similar effect was observed for the solutions of charged polyelectrolytes (Stone and Bradley, 1967). A complex view of the effect of the layer charge also involves an enhancement of the ionic strength in zones near the particle surface, including the electrical double layer. The complex character of this phenomenon relates to the complicated and not fully understood mechanisms of all the processes involved. Although the adsorption of dye cations on the clay mineral surface is a very fast diffusion-limited process (Hsu *et al.*, 1997; Gemeay, 2002; Baranyaiová and Bujdák, 2016), relatively slow processes are also involved in the formation and/or rearrangement of dye molecular assemblies (Gessner *et al.*, 1994; Neumann *et al.*, 1996; Cione *et al.*, 1998). A detailed characterization of these processes would help to understand the reaction mechanisms of dye molecular aggregation in clay colloids (Chaudhuri *et al.*, 2000). By understanding the mechanisms, one could identify the relationships between the properties of the clay-mineral particle surface and the spectral responses of metachromatic dyes (Baranyaiová and Bujdák, 2016). This knowledge could be applied to similar systems based on other organic cations or the colloids of other layered

https://doi.org/10.1346/CCMN.2018.064089 Published online by Cambridge University Press

compounds. Recently, detailed analysis of dye aggregation reaction kinetics and the use of chemometric methods have enabled the analysis of several processes involved in the interactions of rhodamine 123 (R123) (Baranyaiová and Bujdák, 2016) and rhodamine 6G (Lofaj *et al.*, 2013).

One of the most commonly investigated parameters in dye molecular aggregation is dye surface concentration. The positive effect of this parameter on dye aggregation has been reported for various types of metachromatic dyes, *e.g.* MB (Schoonheydt and Heughebaert, 1992) or xanthene dyes (Estevez *et al.*, 1993, 1994). Dye molecular aggregation is not limited to large dye loadings. Large amounts of dye aggregates can be formed even at very low loadings (Estevez *et al.*, 1994). Smectites with high charge densities efficiently induce dye aggregation under a variety of conditions (Bujdák, 2006). The effect of dye loading on changes over time has not been studied systematically.

The objective of the present work was to shed more light on the effects of dye surface concentration on dynamic processes in the molecular aggregation of R123 in montmorillonite colloidal dispersions. The average surface concentration of R123, controlled by the dye/clay mineral ratio, controls the distances between adsorbed dye molecules. The effects of dye surface concentration on the course and reaction kinetic aspects of this phenomenon are described for the first time.

MATERIALS AND METHODS

Chemicals and materials

Rhodamine 123 chloride salt was purchased at laser-grade purity from Sigma-Aldrich (Steinheim, Germany). The structural formula of the R123 cation is shown in Figure 2. Hexadecyltrimethyl ammonium (HDTMA) bromide ($\geqslant$99%) was also purchased from Sigma-Aldrich. The Na^+-form of montmorillonite Kunipia F (MntK), purchased from Kunimine Industries Co., Ltd. (Tokyo, Japan), was used as received without any pretreatment; its structural formula was determined previously (Hrachová *et al.*, 2009):

$$Na_{0.84}Ca_{0.05}K_{0.01}[Si_{7.82}Al_{0.18}][Al_{3.19}Fe_{0.21}Mg_{0.52}]O_{20}(OH)_4$$

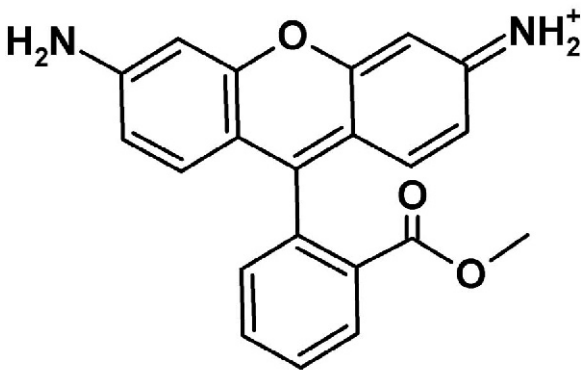

Figure 2. Structural formula of the rhodamine 123 cation.

Dye solutions and MntK colloidal dispersions were prepared using deionized water purified with a Millipore Milli-Q water system from Merck (Darmstadt, Germany). Isopropanol and ethanol were purchased at spectral purity from Slavus (Bratislava, Slovakia). Silver nitrate (>99.8%) was purchased from Centralchem (Bratislava, Slovakia).

Determination of the cation exchange capacity (CEC)

The method of determining the CEC was based on the exchange of inorganic cations with HDTMA. The solution of HDTMA bromide was prepared in a mixture of water and isopropyl alcohol (1:1 (v/v)). The HDTMA in an amount in excess of the expected CEC value (~2 mmol g^{-1}) was added slowly to the aqueous dispersion of MntK and stirred at 50ºC for 3 h. The excess HDTMA bromide solution from the organoclay suspension was removed by centrifugation and washing with a solution of water and isopropyl alcohol (1:1 (v/v)). The washing was repeated several times until the reaction of the supernatant to $AgNO_3$ solution was negative. The purified organoclay was separated by centrifugation, dried at 50ºC, and ground in a mortar. The amount of carbon in the sample was determined using an EMIA-320 V2 AC C/S analyzer (Horiba Scientific, Kyoto, Japan) and used to calculate the CEC which was then corrected to the weight of the dried MntK. The fraction of adsorbed water in MntK was determined by thermogravimetry, performed using a TA Instruments SDT 2060 system (New Castle, Delaware, USA). A small amount of MntK sample was heated from 25 to 500ºC in air at a heating rate of 10ºC min^{-1}.

Preparation of samples

An aqueous solution of R123 was prepared by dissolving a small amount of the dye in deionized water. The stock solution of the dye was standardized spectroscopically: after an appropriate dilution of the stock solution in ethanol, absorption spectra of R123 were measured and the R123 concentration was determined according to the Beer-Lambert law, taking into account the molar absorption coefficient of R123 in ethanol (ε_{512} = 8.52×10^4 mol^{-1} dm^3 cm^{-1} (Du *et al.*, 1998)). An aqueous solution of R123 (1.67×10^{-5} mol dm^{-3}) was prepared and used for reaction kinetics measurements. Colloidal dispersions of MntK were prepared by dispersing the required amount of MntK in water, homogenizing with ultrasound, and stirring overnight. For each measurement, freshly prepared colloids were prepared and used within 48 h. Perfectly delaminated MntK particles, due to the very low concentration of colloidal dispersions, were expected. Light scattering from MntK colloids did not change significantly over the timescale used for the spectral measurements. The final concentration of R123 in

https://doi.org/10.1346/CCMN.2018.064089 Published online by Cambridge University Press

Table 1. Compositions of mixtures used for reaction-kinetics measurements.

c_{MntK} (g dm^{-3})	n_{R123}/m_{MntK} (mmol g^{-1})	n_{R123}/m_{MntK} (%CEC)
4.18×10^{-1}	0.02	1.75
1.67×10^{-1}	0.05	4.37
1.19×10^{-1}	0.07	6.11
6.96×10^{-2}	0.12	10.5
5.57×10^{-2}	0.15	13.1
4.19×10^{-2}	0.20	17.4
3.35×10^{-2}	0.25	21.8
1.68×10^{-2}	0.50	43.6
8.38×10^{-3}	1.00	87.2

c_{R123} was always 8.35×10^{-6} mol dm^{-3}. The experimentally determined value of the CEC of MntK was 1.14 mmol g^{-1}. The symbols c, n, and m denote the concentration, amount, and mass of substance, respectively.

the reaction mixtures was always 8.35×10^{-6} mol dm^{-3}. The R123/MntK ratio (n_{R123}/m_{MntK}) was altered by changing the MntK concentration, which was in the range 4.18×10^{-1} to 8.38×10^{-3} g dm^{-3}. The values were corrected to the weight of dry MntK sample obtained by thermogravimetric measurements. The final range for the R123/MntK ratio was between 0.02 and 1.00 mmol g^{-1} (Table 1).

Reaction kinetics measurements

The mixing of the reactants was performed using an RX2000 Rapid Mixing Stopped-Flow Unit (Applied Photophysics Ltd., Leatherhead, UK). An aqueous solution of R123 and MntK colloid was mixed in a 1:1 ratio (v/v). The temperature of the reactants was adjusted to 25ºC before the reaction. The same temperature was set in the stopped-flow device and in the thermostated cell holder (89054A, Agilent Technologies, Waldbronn, Germany). A stopped-flow device with a quartz cell of path length 10 mm was connected to an Agilent 8453 UV-Vis spectrophotometer (Agilent Technologies, Waldbronn, Germany) equipped with a diode array detector that enabled very quick sampling of spectra (<1 s for the entire spectrum). The reactions were initiated by a trigger upon injecting the reactants into the cell, and the collection of the spectra was controlled by the software in the spectrophotometer (Agilent UV-Vis ChemStation, Agilent Technologies, Waldbronn, Germany). Absorption spectra were measured in kinetics mode over the entire wavelength range. Spectral changes of R123 in MntK colloidal dispersions were recorded in three measurements. For each reaction mixture, measurements were made for 120 s, 10 min, and 3 h.

Chemometric analysis of spectral data

The chemometric analysis was performed for a selected wavelength range of 400 to 600 nm. Multivariate curve resolution (MCR)-alternating least squares and principal component analysis (PCA) were applied with the software *Unscrambler* (CAMO Software, Oslo, Norway). Detailed information on the chemometric methods has been published elsewhere (Lofaj *et al.*, 2013). Baseline correction of the spectra was done before the calculations. Chemometric calculations were performed on data from reactions lasting 120 s and 3 h. The PCA calculation was performed for mean-centered spectral data arranged in a matrix, with a model test of random cross-validation. For the MCR, non-negativity constraints were applied for both spectra and concentrations. The MCR was able to identify the spectral profiles of the main components and their concentrations at different reaction times. Concentration profiles (c'_{mon}, c'_{aggr}) were represented by relative concentrations of R123 species expressed in arbitrary units. Spectral profiles were represented by the molar absorption coefficients of the dye species (ε'_{mon} and ε'_{aggr}), which are also expressed in arbitrary units. The real concentrations were calculated using a multiple linear regression (MLR) analysis with the software *Origin 2017* (OriginLab Corporation, Northampton, Massachusetts, USA). The relative concentrations of R123 species were fitted to the known sum concentration c_{R123}, using equation 1, with an intercept fixed to zero during the calculation:

$$c_{R123} = r_{mon} \cdot c'_{mon} + r_{aggr} \cdot c'_{aggr} \quad (1)$$

The scalar parameters r_{mon} and r_{aggr} expressed the ratio between real and relative concentrations of R123 species. The real values of concentrations (c_{mon}, c_{aggr}) and molar absorption coefficients (ε_{mon} and ε_{aggr}) were calculated using equations 2 and 3:

$$c_i = r_i \cdot c'_i \quad (2)$$

$$\varepsilon_i = \varepsilon'_i / r_i \quad (3)$$

Where i denotes R123 species, either as aggregates or monomers. The real spectral profiles of R123 species were analyzed in detail. The angle between the transition moments of the R123 cations in dimer or aggregate (α) was calculated using the ratio of the spectral areas assigned to the H- and J-bands ($A_{H\text{-band}}$, $A_{J\text{-band}}$) (equation 4, (Carbonaro, 2011)):

$$\tan^2\left(\frac{\alpha}{2}\right) = \frac{A_{J-band}}{A_{H-band}} \quad (4)$$

Determination of reaction kinetics parameters

The fitting of the real concentration profiles of R123 aggregates was performed using non-linear regression analysis in *Origin 2017*. A two-phase exponential growth model was applied using equation 5:

$$c^{\infty}_{aggr} - c_{aggr} = c_1 \cdot e^{-k_1 \cdot t} + c_2 \cdot e^{-k_2 \cdot t} \quad (5)$$

Parameter c_{aggr} refers to the concentration of R123 cations forming aggregates, which changed over the

https://doi.org/10.1346/CCMN.2018.064089 Published online by Cambridge University Press

course of the reaction. c^{∞}_{aggr} represents the concentration of R123 molecules in aggregated form at infinite time. The rate constants k_1,k_2 were determined from the regression analysis and characterize fast and slow reaction processes. c_1, c_2 are the concentration spans involved in the processes. The concentration of R123 cations forming aggregates at time zero (c^{0}_{aggr}) was calculated using equation 6.

$$c^{0}_{aggr} = c^{\infty}_{aggr} - (c_1 + c_2) \quad (6)$$

Averaged half-lives of the formation of R123 aggregates were calculated as the time required to reach the concentration values $c^{t_{1/2}}_{aggr}$ defined by equation 7.

$$c^{t_{1/2}}_{aggr} = c^{0}_{aggr} + \frac{c^{\infty}_{aggr} - c^{0}_{aggr}}{2} \quad (7)$$

The fractions of R123 cations participating in molecular aggregation at the beginning and end of the reaction (designated p_i and p_f, respectively) were calculated as the ratio of the concentration of R123 cations forming aggregates to the total concentration of R123 in the reaction mixture at 0.5 s and 10,000 s after mixing the reactants (equations 8 and 9).

$$p_i = \frac{c^{0.5\,s}_{aggr}}{c^{0.5\,s}_{mon} + c^{0.5\,s}_{aggr}} \quad (8)$$

$$p_f = \frac{c^{10,000\,s}_{aggr}}{c^{10,000\,s}_{mon} + c^{10,000\,s}_{aggr}} \quad (9)$$

The extent of R123 aggregation between the beginning and the end of the reaction (denoted Δp) was calculated as the difference between the p_i and p_f values (equation 10):

$$\Delta p = (p_f - p_i)\cdot 100\% \quad (10)$$

RESULTS AND DISCUSSION

Basic characterization of the spectra

An aqueous solution of R123 absorbs in the range 400−560 nm with the maximum at 500 nm (Figure 3). The main band was assigned to a $\pi \rightarrow \pi^*$ electronic transition and a weak shoulder at lower energies is probably a 1−0 vibronic component. Significant spectral changes were observed right at the beginning of the reaction: the bathochromic shift to longer wavelengths (507 nm) was observed 0.5 s after mixing R123 solution with MntK dispersion. This change is attributed to the adsorption of dye cations on the surface of MntK particles. The shape of the spectrum remained unchanged and the shift of the main band represented an energy difference of ~280 cm^{-1}. As the reaction progressed, the absorbance of the main band decreased, followed by broadening of the band, mainly toward longer wavelengths. After 10^4 s, absorbance was reduced by ~45% (Figure 3). Such spectral changes can be interpreted by the formation of dye molecular aggregates over the course of the reaction. Similar trends have been observed for this dye in similar systems (Baranyaiová and Bujdák, 2016) and also for other

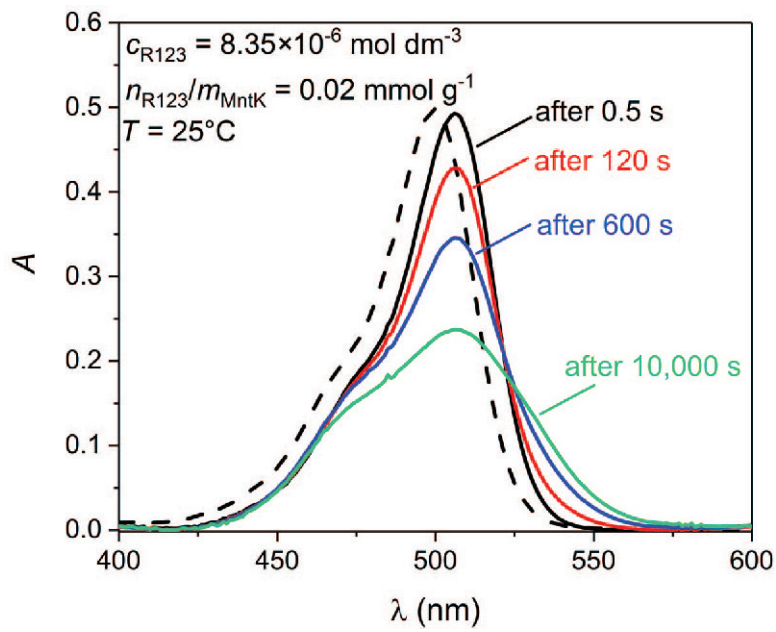

Figure 3. Absorption spectra of R123 in aqueous solution (dashed line) and in colloidal dispersion of MntK recorded during kinetics measurements at various time points after mixing the reaction mixture (solid lines). Spectra were recorded for the mixture at an R123/montmorillonite ratio of 0.02 mmol g^{-1}.

https://doi.org/10.1346/CCMN.2018.064089 Published online by Cambridge University Press

xanthene dyes (Bujdák and Iyi, 2006; Bujdák *et al.*, 2007; Lofaj *et al.*, 2013). The R123/MntK ratio affected significantly the spectral properties of the dye (Figure 4). At the beginning of the reaction (Figure 4, upper part), 0.5 s after mixing the components, the spectra at low dye loadings are similar to those of the dye solution but remain shifted to longer wavelengths, as mentioned above. At higher loadings, especially at 1 mmol g^{-1}, a significant change was observed: a new shoulder at low wavelengths appeared in the spectrum, which can be attributed to H-aggregates. The R123/MntK ratio in this case was close to the CEC of MntK, which means that the Mnt surface was saturated with R123 cations. Under these conditions, dye aggregation was very likely. In addition, partial destabilization of the colloid was observed, because the surface charge of the particles was neutralized. At the end of the reaction (Figure 4, lower), the spectra of the systems with lower dye loadings also exhibited significant dye aggregation. Dispersions with the lowest R123/MntK ratio exhibited an obvious broadening of the spectral band, more than observed for systems with medium dye loadings. A qualitative estimate of the trends in the spectra over time or the effect of dye/MntK ratio is not sufficient to interpret the effect of these parameters or the mechanisms of the reactions. Chemometric analysis of the spectra was performed to shed more light on these aspects.

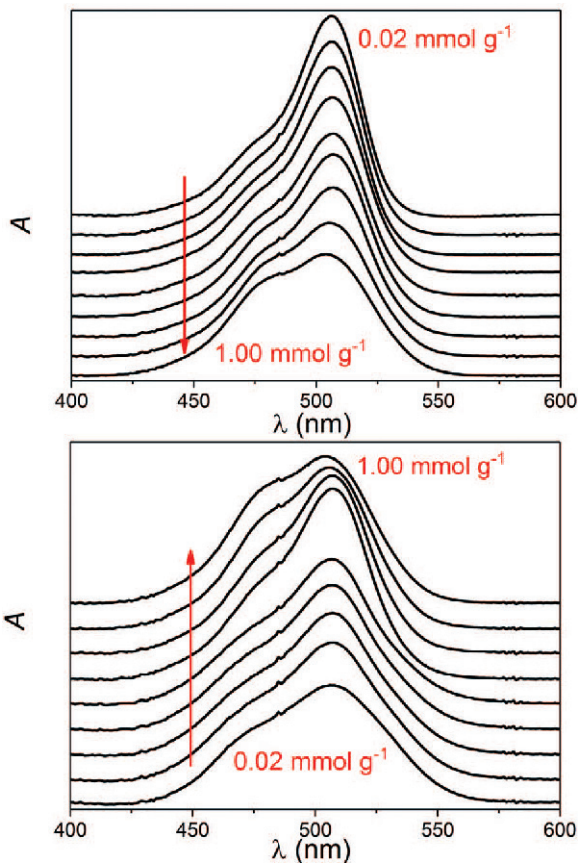

Figure 4. Effect of dye/montmorillonite ratio on absorption spectra of R123 in MntK colloids. The spectra were recorded 0.5 s (upper) and 3 h (lower) after mixing the reactants. Arrows in the figures indicate the direction in which the value of the dye/montmorillonite ratio increases. The spectra were shifted vertically to provide more clarity.

Chemometric analysis

The MCR was performed to calculate the vectors of spectral profiles of the most relevant components and sample concentrations. The most significant components selected should be able to explain all measured spectra with sufficiently low residuals. The baselines had to be corrected in order to achieve reliable results. The spectral range was reduced to avoid the influence of non-significant wavelengths outside the range of the dominant spectral absorption. In addition to the non-negativity constraints for both the spectra and the concentrations used in the MCR calculation; the relevance and number of spectral components representing all measured spectra were decided. Calculated spectral profiles must be realistic when determining the number of relevant spectral components. The spectrum of adsorbed monomers may be shifted slightly from that of the dye solution, but its spectral profile was considered to be similar to that of the dye solution. In fact, taking into account the two main spectral components (Figure 5), the absorption spectrum of monomers calculated by MCR was very similar to that of the dye solution (Figure 3, dashed line). The maximum absorption of monomers as well as some of the spectra recorded at the beginning of the reaction (see spectra in Figures 3 and 4 measured after 0.5 s) were shifted slightly to longer wavelengths. A similar change was

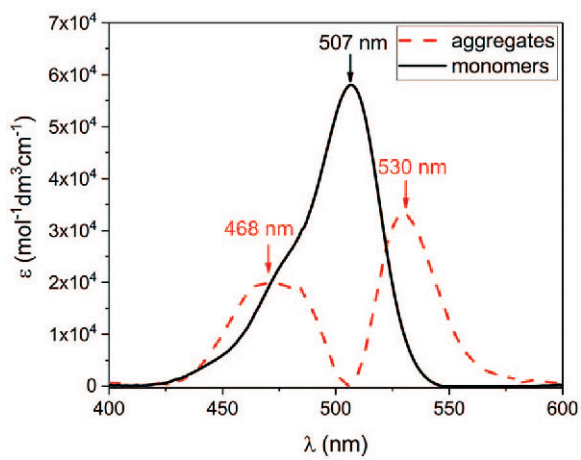

Figure 5. Spectral profiles of R123 monomers (solid line) and molecular aggregates (dashed line) obtained as a result of chemometric analysis using the method of multivariate curve resolution.

https://doi.org/10.1346/CCMN.2018.064089 Published online by Cambridge University Press

observed for colloidal dispersions based on saponite (Baranyaiová and Bujdák, 2016). The second spectral component represented imperfect, so-called 'oblique' J-aggregates with absorptions at wavelengths shorter and longer than those of the monomers (Figure 5, dashed line). The molecular aggregation of R123 led to the splitting of the excitation energy into two new states. Due to the imperfect structure of the aggregates, transition to both the higher- and lower-energy state was allowed (Figure 6a), which was reflected in the appearance of both absorption bands. A somewhat greater intensity and slightly narrower width of the red-shifted absorption band (the so-called J-band) were observed. The energy difference between the H- and J-band was 2500 cm^{-1}. The ratio between the areas of the bands indicates the possible structure of the aggregate. According to the calculation using equation 4, the angle between the transition moments of adjacent R123 cations forming the aggregate was ~95º (Figure 6b). A further increase in the number of spectral components calculated by the MCR method resulted in the spectra of monomers and two types of aggregates (Supplemental Materials section, deposited with the Editor in Chief and available at https://www.clays.org/Journal/JournalDeposits.html, Figure SM1). The large spectral overlap of the species probably leads to an erroneous estimate of spectral profiles and concentrations when the number of components is high. The sensitivity limit of the spectrophotometer used makes the correct identification of the third component impossible if it is present in relatively small amounts, if its spectral profile is similar to other species, or if significant spectral overlap exists between the species. The two-component model, therefore, provided the most realistic results for further quantitative analysis, and the third component could only be considered qualitatively. The PCA model performed for the mean-centered spectra resulted in two PCA components representing an optimal number of three linearly uncorrelated spectral species. The explained variances for the two- and one-PCA component models were 98.4% and 95.3%, respectively. Both numbers represent a statistically significant value. Potential outliers identified by the PCA model were assigned to the samples represented by the lowest dye loading (0.02 mmol g^{-1}), especially those found in the first few seconds of the reaction (not shown). Another type of outlier from the PCA model were the spectra obtained at the end of the reaction. A decreasing stability of the colloidal dispersions could be the cause of the deviation of the spectra from the model. The relevance

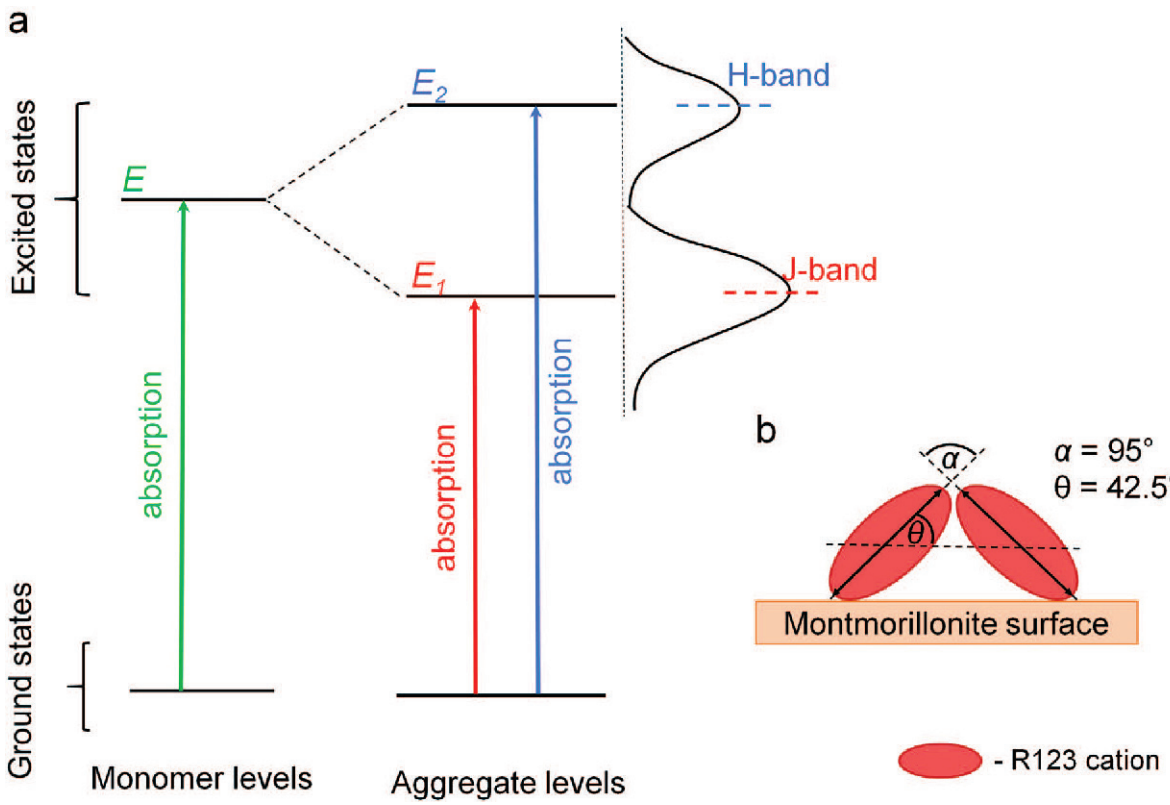

Figure 6. Splitting of the energy of the excited state of R123 aggregate into lower (E_1) and higher (E_2) states (a). Schematic illustration of mutual arrangement of R123 molecules in oblique head-to-tail aggregate (b). The α symbol corresponds to the angle between the transition moments of R123 cations in the aggregate (marked with double-headed arrows). The symbol θ indicates the slip angle. The dashed line corresponds to the centerline of the interacting molecules of R123.

https://doi.org/10.1346/CCMN.2018.064089 Published online by Cambridge University Press

of the third component was also estimated by comparing the variable residuals obtained by the MCR method. Although the variable residuals also exhibited structured spectral profiles in addition to spectral noise, the absorbance values obtained were well below 0.01. The residuals represented ~1−2% of the absorbance of the real spectra. Increasing the number of components from two to three did not change significantly the variable residuals (Figure SM2). Sample residuals for both cases were also considered and compared. The values were almost negligible, to the same extent as was observed for the variable residuals, but they exhibited an interesting structure that had peaks for the spectra recorded at the beginning of the reaction. Such a trend could indicate a more complex nature of the colloidal system formed immediately after mixing the reactants. Dye molecules can form intermediate, unstable aggregates, which then convert to a more stable form within a short time. To shed more light on the mechanism, the differences between the sample residuals were analyzed in detail, considering two and three components (Figure 7). Interestingly, both reaction progress and dye loading played an essential role in describing the spectra with the model of two or three species. Obviously, the largest difference between the model taking into account two or three components was observed at the beginning of the reactions at low dye loadings (0.02−0.07 mmol g^{-1}) (Figure 7). Note that the difference is very small ΔA = 0.002−0.004. As the reaction progressed, the difference decreased significantly at the end of the reaction to <0.001. For the samples with higher dye loadings, the difference is close to zero and represents an absorbance of 0.0005−0.0015. The structure of the sample residuals can be interpreted in two ways:

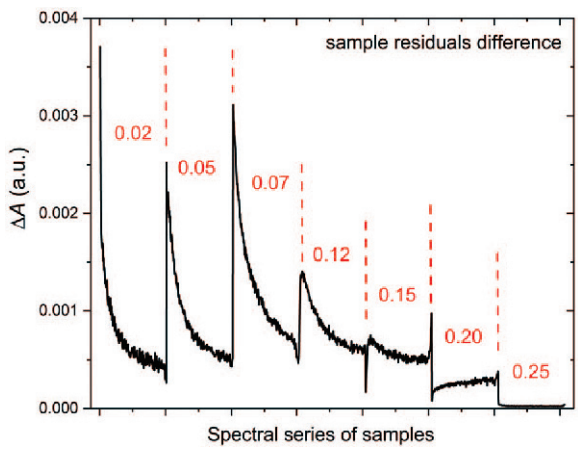

Figure 7. Comparison of difference between sample residuals obtained for two- and three-spectral component systems for investigated reaction systems of R123 and MntK. The plots show the evolution of the function over reaction time. Sample residuals for two and three spectral components of R123 were achieved as the result of calculations using the multivariate curve resolution method. The curves assigned to the individual reaction systems are arranged in succession for better clarity. The labels 0.02−0.25 correspond to the specific dye/montmorillonite ratio (in mmol g^{-1}). The label on the horizontal axis corresponds to the absorption spectra recorded during the kinetic measurement of R123 molecular aggregation.

(1) Three or more components were present in the systems at the beginning of the reaction, but mostly in the dispersions of low dye loadings. These components were formed at very low concentrations and could have similar spectral properties that are barely recognized by the method.

(2) A slight variation in the structure of the aggregates occurred during the course of the reaction. The aggregates formed at the beginning of the reaction could be an intermediate form of those produced at the end of the reaction. The third component, obtained through the MCR analysis, caught our attention; and the spectra of all three components were compared (Figure SM1). The third component was probably a dimer of R123. This assignment is supported by the much lower splitting of the energies of the H- and J-bands (1600 cm^{-1}). The dimer also exhibited a slightly different structure with a J-band of much greater intensity than the H-band, indicating a slightly larger angle between the transition moments of the molecules assembled in the dimers. According to the calculation using equation 4, the angle could be 128º. All these facts should be considered to be qualitative information because the spectra of all three species overlap significantly which may affect the accuracy of the spectral-profile calculation. Another interesting feature of the third component is its concentration, which in most systems changed little over time (Figure SM3), and this is in contrast to most concentration profiles of dye monomers or aggregates. This is a typical feature for consecutive reactions with a steady state for an intermediate, which reflects the balance between the amounts of intermediate molecules formed and decomposed.

Reaction kinetics. The proposed model of the reaction mechanism takes into account the presence of two species, dye monomers and one type of molecular aggregate. The two-component system was considered in a simplified approach, in which the formation of 'oblique' J-aggregates occurs through the association of dye molecules. Non-linear regression analysis was applied for the concentration profiles of R123 cations involved in aggregation. Regression analysis was performed on the data obtained from 3 h of measurements. The first- and second-order reaction kinetics models were unable to describe concentration profiles of R123 aggregates (not shown). Other, more complex models were taken from other studies aimed at the formation of dye molecular aggregates in heterogeneous systems, in solutions of electrolytes, *etc*. The first model uses first-order reaction kinetics with time-dependent rate constants. In this case, the profile follows the increasing concentration of dye molecular aggregates of

https://doi.org/10.1346/CCMN.2018.064089 Published online by Cambridge University Press

a stretched exponential function. This model captures the complex character of dye molecular aggregation, and has been used for the kinetics of the molecular aggregation of rhodamine 6G in montmorillonite colloids (Lofaj *et al.*, 2013), and for the salt-induced aggregation of thiacarbocyanine dye in aqueous solution (Chibisov *et al.*, 2004).

The second model is based on a two-phase exponential function. This model was proposed to describe the kinetics of molecular aggregation of thiacyanine dye on the surface of noble metal nanoparticles (Vujačić *et al.*, 2012) and in the molecular aggregation of rhodamine 123 in colloids of synthetic saponite particles (Baranyaiová and Bujdák, 2016). According to the results of the non-linear regression analysis, the model based on a two-phase exponential function (using equation 5) fitted more closely with the concentration profiles. The values for the coefficient of determination were higher when using the two-phase exponential function ($R^2 > 0.99$) than when the fits were based on models with a time-dependent rate constant. In a residual plot, small deviations from the model of the two-phase exponential function over the entire time range were observed. The distribution of the residuals was structureless and irregular (Figure SM4a). Using the time-dependent rate constant model, larger residuals were obtained, especially for data obtained for longer reaction times. The regression residuals in this case exhibited structured profiles, suggesting that the trends in data did not follow the model using a stretched exponential function (Figure SM4 b). The more accurate model, based on two-phase exponential growth, simulates the formation of R123 molecular aggregates in two parallel processes, both of which follow first-order reaction kinetics. Faster and slower processes of R123 molecular aggregation were the two different reactions that were independent of each other (Figure 8). These reactions can be characterized by rate constants k_1 and k_2, respectively. Parallel processes with different rate constants can indicate the presence of different active sites on the surface of MntK particles, which have variable catalytic efficiency to promote the formation of R123 aggregates (Baranyaiová and Bujdák, 2016). The model based on two catalytically different sites proved to be suitable for describing the measured data.

The time evolution of the concentration of R123 cations that formed molecular aggregates during the first 1000 s was analyzed in detail (Figure 9). The colloidal dispersions with low surface concentrations of R123 exhibited a relatively slow formation of dye aggregates. The dispersion with the lowest R123/MntK ratio required ~30 s before the first aggregates were detectable. Other systems contained dye aggregates at the beginning of the reaction, which were clearly detected in the first recorded spectrum. The concentration of dye molecules involved in the instantaneous formation of the aggregates increased significantly with dye loading, giving values of 0.11−1.60 μmol dm^{-3} for the dispersions, with R123

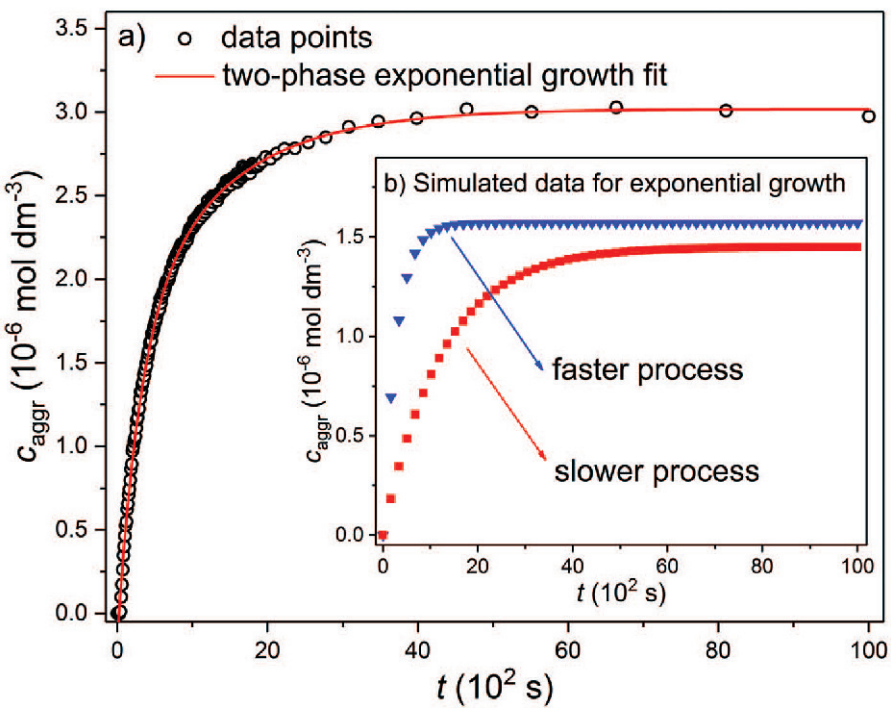

Figure 8. Two-phase exponential growth fit applied to a concentration profile of R123 cations forming molecular aggregates in a reaction mixture with a R123/montmorillonite ratio of 0.02 mmol g^{-1}. Curve fitting was done using equation 5 (a). Simulated curves for processes involved in the formation of R123 molecular aggregates (b).

https://doi.org/10.1346/CCMN.2018.064089 Published online by Cambridge University Press

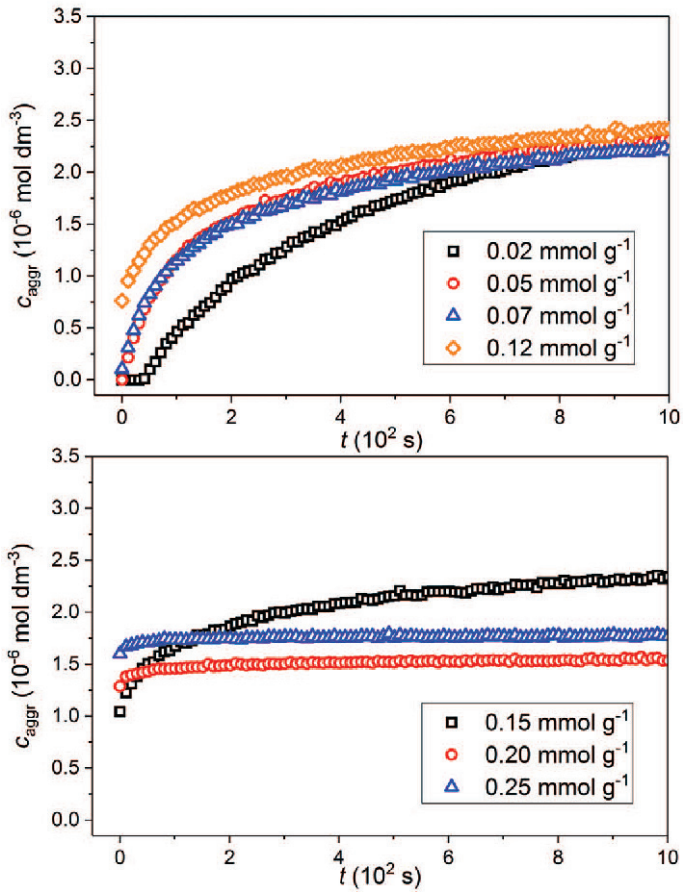

Figure 9. Evolution of the concentration of R123 cations that formed molecular aggregates over time, depending on the dye/montmorillonite ratio, over a shorter timescale.

loading of 0.05 to 0.25 mmol g^{-1} (Table 2). The colloids with high loadings (0.50 and 1.00 mmol g^{-1}) were also measured, but were not involved in the chemometric analysis. Low stability of the colloidal dispersions, flocculation, and large light scattering were observed. Presumably, the adsorption of large amounts of dye cations significantly neutralized the surface charge, thereby minimizing the electrostatic stabilization of MntK colloidal particles (Garfinkel-Shweky and Yariv, 1995). The rapid, almost instantaneous formation of the aggregates at a high surface concentration is characterized by the parameter c^0_{aggr} (Table 2). As was mentioned above, all concentration profiles determined from the chemometric analysis were fitted to biphasic exponential

Table 2. Parameters of reaction kinetics of R123 molecular aggregation obtained using a two-phase exponential growth function for systems with variable dye/montmorillonite ratios.

n_{R123}/m_{MntK} (mmol g^{-1})	$c^0_{aggr}/c^\infty_{aggr}$ (μmol dm^{-3})	k_1/k_2 (10^{-3} s^{-1})	$t_{1/2}$ (s)	Δp %
0.02	0.0/3.02	3.44/0.80	356	42
0.05	0.110/2.91	9.25/0.74	182	39
0.07	0.210/2.71	9.68/0.89	178	35
0.12	0.848/2.70	9.96/1.19	178	26
0.15	1.11/2.48	13.8/1.67	146	20
0.20	1.31/1.57	26.4/1.39	50.5	3.9
0.25	1.60/1.77	50.6/3.70	19.5	2.5

c^0_{aggr}, c^∞_{aggr}: calculated concentrations of dye molecules forming aggregates at the beginning and at the end of the reaction; k_1, k_2: rate constants for the fast and slow reaction process, respectively; $t_{1/2}$: half-life; Δp: the extent of the dye aggregation between the start and the end of the reaction.

https://doi.org/10.1346/CCMN.2018.064089 Published online by Cambridge University Press

functions. The growth of the aggregate concentration did not obey simple reaction kinetics. Two parallel reactions had to be considered to describe the change in concentration over time. The fits considering two parallel reactions resulted in two rate constants (for the faster and slower reaction) and average half-lives. The parameters determined for the formation of molecular aggregates are summarized in Table 2. The increasing rate constant of the faster reaction of 3.44×10^{-3} to 50.6×10^{-3} s^{-1} with an increasing dye loading of 0.02−0.25 mmol g^{-1} demonstrated clearly the relationship between reaction kinetics and dye surface concentration. The reaction rate for a slower reaction at a loading of 0.25 mmol g^{-1} reached a similar value ($k_2 = 3.70 \times 10^{-3}$ s^{-1}) to the higher rate constant for dye loading of 0.02 mmol g^{-1} ($k_1 = 3.44 \times 10^{-3}$ s^{-1}). With an increase in R123 loading, the total half-life decreased from 356 to 19.5 s.

Another interesting aspect of R123 aggregation must be considered. Although relatively large amounts of dye aggregates were formed at the beginning of the reaction at high surface concentrations, the reaction failed to progress further. In fact, for systems with dye surface concentrations of 0.20 and 0.25 mmol g^{-1}, the amount of dye aggregates did not change after 100 s of reaction. Colloidal dispersions of lower dye loadings initially contained much smaller amounts of dye aggregates, but the aggregation continued. The amount of dye molecules that form aggregates in the colloidal dispersion with an R123/MntK ratio of 0.15 mmol g^{-1} gradually exceeded the levels in other systems with greater dye surface concentrations that occurred during relatively short reaction times. In addition, the dispersion of the lowest dye loading (0.02 mmol g^{-1}) formed the largest amount of dye aggregates at the end of the reaction (Figure 10). For time extrapolated to infinity, 42% of the dye molecules formed aggregates (Table 2). Although initially a relatively large amount of dye aggregates was formed in the colloid with 0.25 mmol g^{-1} loading, only a 2.5% change between the beginning and end of the reaction was observed. These facts show significantly different properties between the systems compared. The greater dye:smectite ratios resulted in the rapid formation of dye aggregates which were likely to be relatively stable, and underwent no further changes observable by absorption spectroscopy. More interestingly, monomers that remained coexistent with the dye aggregates in these

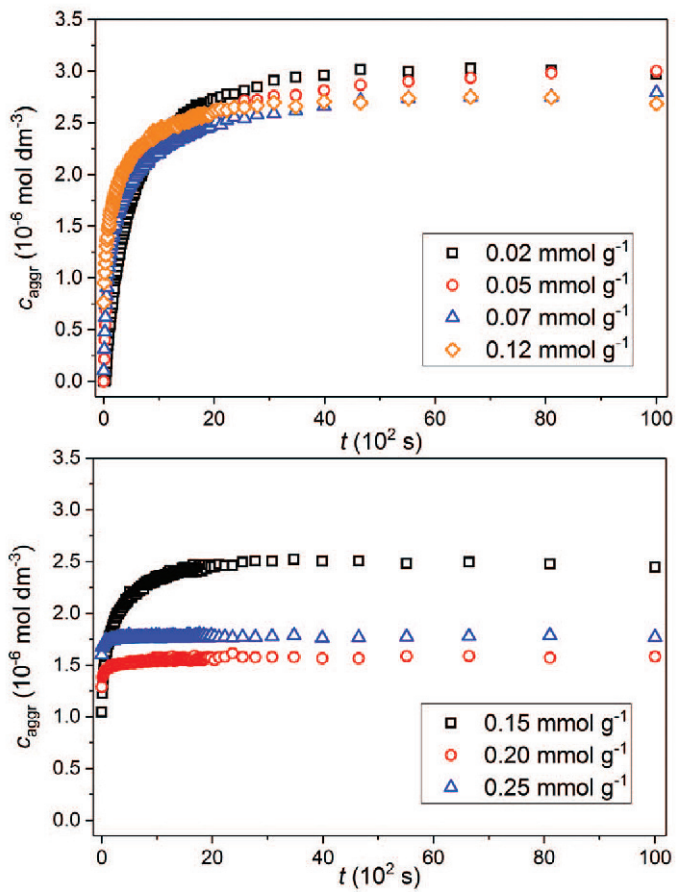

Figure 10. Evolution of the concentration of R123 cations that formed molecular aggregates over time, depending on dye/montmorillonite ratio, over a longer timescale.

https://doi.org/10.1346/CCMN.2018.064089 Published online by Cambridge University Press

colloidal dispersions also did not change with reaction time. This is in contrast to the systems with low dye loadings, where monomers exhibited a strong tendency to aggregation over time. Such a difference can be explained by the rapid kinetics that occur in the adsorption process (Gemeay, 2002). Under conditions of perfectly exfoliated smectite particles, the rate of the adsorption process can be limited by the diffusion rate of the molecules, which can be close to 10^9 mol dm^{-3} s^{-1} for aqueous systems. At such a large rate, dye molecules would initially be adsorbed heterogeneously onto the fraction of particles they encounter first. The diffusion and rapid adsorption of dye cations would be terminated before complete mixing with smectite particles is achieved. A fraction of the particles occupied with dye cations would be neutralized by positive charge from the dye cations, which could lead to an association between the MntK particles. The association could lead to a trapping of the aggregates formed, but also prevents further reaction of the remaining monomers. Increased scattering and flocculation of the particles was observed visually for the systems with the greatest dye loadings, such as 0.50 and 1.00 mmol g^{-1}, but probably also occurred to some extent in the dye loadings of 0.20 and 0.25 mmol g^{-1}. On the other hand, the properties of the hybrid systems were significantly different at the lowest dye loadings. No significant neutralization of the charge occurred. Although no aggregates were formed initially, dye monomers could migrate freely on the surface of the particles to form dimers or larger aggregates over time. Dye aggregation at high loadings was promoted by the reaction kinetics. Aggregation at low dye loadings was controlled thermodynamically and the reaction rates were slow (see Table 2). The thermodynamically controlled aggregation probably occurred at the sites that promote this reaction, such as the zones of large layer-charge density. Systems based on a low loading are assumed to be a better choice for characterizing the surface properties of clay minerals with metachromatic dyes. The trends observed for the growth of molecular aggregates were reflected in the decrease in the concentration of R123 monomers over time (Figures SM5, SM6). The dispersions with the greatest dye loadings were already characterized in the first few seconds of the reaction with a reduced concentration of monomers (Figure SM6). On the other hand, the reaction did not proceed and the concentration of monomers did not change with time. The systems with low dye loadings were characterized by a slow decrease in the monomer concentration but at the end of the reaction reached a relatively large decrease in concentration (Figure SM5).

CONCLUSIONS

The chemometric analysis of the spectra of R123 in colloidal dispersions of MntK provided detailed information on possible spectral and structural properties of the dye aggregates formed. The time dependence of the concentration of R123 aggregates helped to identify possible reaction mechanisms. The aggregation of dye molecules at the colloidal particle interface is a relatively complicated process that depends on the thermodynamics of dye dimerization and aggregation, the stability of dye molecular aggregates, and the reaction kinetics of the process. Dye aggregation can be influenced by altering the properties of colloidal particles upon neutralization of their charge by dye cations. Rhodamine 123 exhibits a very rapid adsorption onto montmorillonite particles, which is probably only limited by diffusion. On the other hand, the formation of dye molecular aggregates is much more complicated and depends on the dye/montmorillonite ratio. In dispersions with high rhodamine 123/montmorillonite ratios, relatively large amounts of dye molecular aggregates were formed, which had already been detected after the first few seconds of the reaction. The formation of dye molecular aggregates at low dye loadings was relatively very slow, but achieved high yields after longer reaction times. On the other hand, the systems with high dye loadings exhibited spectral equilibrium immediately after mixing the components, and the amount of aggregates formed did not change significantly with time. The association between montmorillonite particles, which was promoted by dye adsorption, probably played a significant role in this phenomenon. The present study has demonstrated the complex nature of systems based on colloids of organic dyes and clay minerals. This knowledge can be extrapolated to some aspects of the interaction between clays and organic compounds in general or to the phenomena that occur in reactions with other layered nanomaterials.

ACKNOWLEDGMENTS

The present work was supported by the Slovak Research and Development Agency under contract No. APVV-15-0347 and APVV-15-0741. Support from the VEGA grant agency (1/0278/16, 2/0141/17) and from Comenius University in Bratislava (UK/227/2016) is also acknowledged gratefully. The authors thank Associate Professor Milan Drábik of the Department of Inorganic Chemistry in Comenius University in Bratislava for making it possible to conduct thermogravimetry measurements.

REFERENCES

Baranyaiová, T. and Bujdák, J. (2016) Reaction kinetics of molecular aggregation of rhodamine 123 in colloids with synthetic saponite nanoparticles. *Applied Clay Science*, **134**, 103–109.

Bergmann, K. and O'Konski, C.T. (1963) A spectroscopic study of methylene blue monomer, dimer, and complexes with montmorillonite. *Journal of Physical Chemistry*, **67**, 2169–2177.

Bujdák, J. (2006) Effect of the layer charge of clay minerals on optical properties of organic dyes. A review. *Applied Clay Science*, **34**, 58–73.

Bujdák, J. and Iyi, N. (2006) Molecular aggregation of rhodamine dyes in dispersions of layered silicates:

https://doi.org/10.1346/CCMN.2018.064089 Published online by Cambridge University Press

Influence of dye molecular structure and silicate properties. *Journal of Physical Chemistry B*, **110**, 2180–2186.

Bujdák, J. and Komadel, P. (1997) Interaction of methylene blue with reduced charge montmorillonite. *Journal of Physical Chemistry B*, **101**, 9065–9068.

Bujdák, J., Janek, M., Madejová, J., and Komadel, P. (2001) Methylene blue interactions with reduced-charge smectites. *Clays and Clay Minerals*, **49**, 244–254.

Bujdák, J., Iyi, N., and Fujita, T. (2002) The aggregation of methylene blue in montmorillonite dispersions. *Clay Minerals*, **37**, 121–133.

Bujdák, J., Iyi, N., and Sasai, R. (2004) Spectral properties, formation of dye molecular aggregates, and reactions in rhodamine 6G/layered silicate dispersions. *Journal of Physical Chemistry B*, **108**, 4470–4477.

Bujdák, J., Martinez, V.M., Arbeloa, F.L., and Iyi, N. (2007) Spectral properties of rhodamine 3B adsorbed on the surface of montmorillonites with variable layer charge. *Langmuir*, **23**, 1851–1859.

Carbonaro, C.M. (2011) Tuning the formation of aggregates in silica-Rhodamine 6G hybrids by thermal treatment. *Journal of Photochemistry and Photobiology A – Chemistry*, **222**, 56–63.

Cenens, J. and Schoonheydt, R.A. (1988) Visible spectroscopy of methylene blue on hectorite, Laponite B, and Barasym in aqueous suspension. *Clays and Clay Minerals*, **36**, 214–224.

Chaudhuri, R., Arbeloa, F.L., and Arbeloa, I.L. (2000) Spectroscopic characterization of the adsorption of rhodamine 3B in hectorite. *Langmuir*, **16**, 1285–1291.

Chibisov, A.K., Gorner, H., and Slavnova, T.D. (2004) Kinetics of salt-induced J-aggregation of an anionic thiacarbocyanine dye in aqueous solution. *Chemical Physics Letters*, **390**, 240–245.

Cione, A.P.P., Neumann, M.G., and Gessner, F. (1998) Time-dependent spectrophotometric study of the interaction of basic dyes with clays – III. Mixed dye aggregates on SWy-1 and Laponite. *Journal of Colloid and Interface Science*, **198**, 106–112.

Czímerová, A., Jankovič, L., and Bujdák, J. (2004) Effect of the exchangeable cations on the spectral properties of methylene blue in clay dispersions. *Journal of Colloid and Interface Science*, **274**, 126–132.

Czímerová, A., Bujdák, J., and Dohrmann, R. (2006) Traditional and novel methods for estimating the layer charge of smectites. *Applied Clay Science*, **34**, 2–13.

Czímerová, A., Čeklovský, A., and Bujdák, J. (2009) Interaction of montmorillonite with phenothiazine dyes and pyronin in aqueous dispersions: A visible spectroscopy study. *Central European Journal of Chemistry*, **7**, 343–353.

Du, H., Fuh, R.-C.A., Li, J., Corkan, L.A., and Lindsey, J.S. (1998) PhotochemCAD: A Computer-Aided Design and Research Tool in Photochemistry. *Photochemistry and Photobiology*, **68**, 141–142.

Epelde-Elezcano, N., Martínez-Martínez, V., Duque-Redondo, E., Temiño, I., Manzano, H., and López-Arbeloa, I. (2016) Strategies for modulating the luminescence properties of pyronin y dye-clay films: An experimental and theoretical study. *Physical Chemistry Chemical Physics*, **18**, 8730–8738.

Estevez, M.J.T., Arbeloa, F.L., Arbeloa, T.L., and Arbeloa, I.L. (1993) Absorption and fluorescence properties of rhodamine 6G adsorbed on aqueous suspensions of Wyoming montmorillonite. *Langmuir*, **9**, 3629–3634.

Estevez, M.J.T., López Arbeloa, F., López Arbeloa, T., López Arbeloa, I., and Schoonheydt, R.A. (1994) Spectroscopic study of the adsorption of rhodamine 6G on laponite B for low loadings *Clay Minerals*, **29**, 105–113.

Garfinkel-Shweky, D. and Yariv, S. (1995) The effect of the exchangeable metallic cation on the colloid properties of laponite treated with acridine orange. A spectrophotometric study. *Colloid and Polymer Science*, **273**, 453–463.

Gemeay, A.H. (2002) Adsorption characteristics and the kinetics of the cation exchange of rhodamine-6G with Na^+-montmorillonite. *Journal of Colloid and Interface Science*, **251**, 235–241.

Gessner, F., Schmitt, C.C., and Neumann, M.G. (1994) Time-dependent spectrophotometric study of the interaction of basic dyes with clays. 1. Methylene-Blue and Neutral Red on montmorrillonite and hectorite. *Langmuir*, **10**, 3749–3753.

Holmes, W.C. (1926) The chemical nature of metachromasy. *Biotechnic and Histochemistry*, **1**, 116–122.

Hrachová, J., Chodák, I., and Komadel, P. (2009) Modification and characterization of montmorillonite fillers used in composites with vulcanized natural rubber. *Chemical Papers*, **63**, 55–61.

Hsu, Y.C., Chiang, C.C., and Yu, M.F. (1997) Adsorption behavior of basic dyes on activated clay. *Separation Science and Technology*, **32**, 2513–2534.

Jacobs, K.Y. and Schoonheydt, R.A. (2001) Time dependence of the spectra of methylene blue-clay mineral suspensions. *Langmuir*, **17**, 5150–5155.

Kasha, M., Rawls, H.R., and El-Bayoumi, M.A. (1965) The exciton model in molecular spectroscopy. *Pure and Applied Chemistry*, **11**, 371–392.

Lofaj, M., Valent, I., and Bujdák, J. (2013) Mechanism of rhodamine 6G molecular aggregation in montmorillonite colloid. *Central European Journal of Chemistry*, **11**, 1606–1619.

López Arbeloa, F., Estevez, M.J.T., López Arbeloa, T., and López Arbeloa, I. (1995) Adsorption of rhodamine 6G on saponite. A comparative study with other rhodamine 6G-smectite aqueous suspensions. *Langmuir*, **11**, 3211–3217.

McRae, E.G. and Kasha, M. (1958) Enhancement of phosphorescence ability upon aggregation of dye molecules [6]. *The Journal of Chemical Physics*, **28**, 721–722.

Miyamoto, N., Kawai, R., Kuroda, K., and Ogawa, M. (2000) Adsorption and aggregation of a cationic cyanine dye on layered clay minerals. *Applied Clay Science*, **16**, 161–170.

Neumann, M.G., Schmitt, C.C., and Gessner, F. (1996) Time-dependent spectrophotometric study of the interaction of basic dyes with clays. 2. Thionine on natural and synthetic montmorillonites and hectorites. *Journal of Colloid and Interface Science*, **177**, 495–501.

Neumann, M.G., Gessner, F., Schmitt, C.C., and Sartori, R. (2002) Influence of the layer charge and clay particle size on the interactions between the cationic dye methylene blue and clays in an aqueous suspension. *Journal of Colloid and Interface Science*, **255**, 254–259.

Sartori, R.A., De Morais, L.C., Consolin-Filho, N., Marques, D.D., and Gessner, F. (2011) Adsorption of methylene blue on clay minerals particles: Analysis of the clay particle sizes. *Quimica Nova*, **34**, 584–588.

Schoonheydt, R.A. and Heughebaert, L. (1992) Clay adsorbed dyes: methylene blue on laponite. *Clay Minerals*, **27**, 91–100.

Stone, A.L. and Bradley, D.F. (1967) Aggregation of cationic dyes on acid polysaccharides. I. Spectrophotometric titration with acridine orange and other metachromatic dyes. *BBA – General Subjects*, **148**, 172–192.

Vujačić, A., Vasić, V., Dramićanin, M., Sovilj, S.P., Bibić, N., Hranisavljevic, J., and Wiederrecht, G.P. (2012) Kinetics of J-aggregate formation on the surface of Au nanoparticle colloids. *Journal of Physical Chemistry C*, **116**, 4655–4661.

(*Received 15th October 2017; revised 20 February 2018; Ms. 1225; AE: T. Fujimura*)